Hindawi
Advances in Civil Engineering
Volume 2020, Article ID 8898318, 19 pages
https://doi.org/10.1155/2020/8898318

Research Article

Stability Analysis of the Left Bank Slope of Baihetan Hydropower Station Based on the MF-DFA Method

Haoyu Mao,[1] Min Zhang,[1] Biao Li,[2] and Nuwen Xu [1]

[1]*State Key Laboratory of Hydraulics and Mountain River Engineering, College of Water Resource and Hydropower, Sichuan University, Chengdu, Sichuan 610065, China*
[2]*School of Geoscience and Technology, Southwest Petroleum University, Chengdu, Sichuan 610500, China*

Correspondence should be addressed to Nuwen Xu; xunuwen@scu.edu.cn

Received 27 June 2020; Revised 11 July 2020; Accepted 13 July 2020; Published 31 July 2020

Academic Editor: Hang Lin

Copyright © 2020 Haoyu Mao et al. This is an open access article distributed under the Creative Commons Attribution License, which permits unrestricted use, distribution, and reproduction in any medium, provided the original work is properly cited.

Based on the left bank slope of Baihetan hydropower station in Southwestern China, a high-precision microseismic monitoring system was established. An early warning model of surrounding rock mass deformation and failure based on MF-DFA was proposed. The results showed that the multifractal characteristics of the microseismic and blasting waveform time series in the left bank slope were obvious, and the multifractal spectrum width of the blasting waveform is much larger than that of microseismic waveform. Before the slope cracks increased, the multifractal time-varying response characteristics of microseismic waveform showed strong regularity, which could be regarded as a precursor of surrounding rock mass deformation. Before the deformation and failure of surrounding rock mass, the multifractal spectrum width $\Delta\alpha$ showed an increasing trend while the multifractal spectrum of microseismic waveforms $\Delta f(\alpha)$ presented a decreasing trend, which can be regarded as a precursor of surrounding rock mass deformation; when deformation and failure occurred, $\Delta\alpha$ showed a decreasing trend and $\Delta f(\alpha)$ showed an increasing trend, which can be regarded as a deformation failure period; after the occurrence of deformation and failure, both $\Delta\alpha$ and $\Delta f(\alpha)$ showed a steady trend, and $\Delta f(\alpha)$ would approach to the zero line, which can be regarded as a stable period.

1. Introduction

The monitoring and early warning of high slope instability have always been a research hotspot and difficulty in the field of rock mechanics and engineering [1–3]. The analysis methods of slope stability mainly include the engineering geological analysis method, model testing, numerical simulation methods, limit equilibrium, limit analysis, and reliability analysis method. These methods play an important role in solving the problem of rock slope stability research. Che et al. [4] conducted a series of shaking table physical tests to study the propagation of seismic waves in jointed rock mass and their influence on the stability of rock slope with discontinuous jointed rock slope in high and steep bedding. Griffiths and Fenton [5, 6] first applied the finite element method to the stability analysis of the slope, promoting the development of the finite element method in the slope engineering. Baker and Garber. [7] used variational method to search for the minimum safety factor and its sliding surface. Hungr et al. [8] extended the Janbu method and Bishop method to three dimensions, which improved the calculation accuracy. Sutcliffe et al. [9] discussed the ultimate bearing capacity of jointed rock foundations based on the limit analysis, presented an extensive parametric analysis, and researched the effect of strength properties and joint orientation on the bearing capacity of jointed rock. Xiao-Li and Liu et al. [10] analyzed the reliability of rock slope in the form of stability factor and explored the relationship between probability of failure and mean safety factor.

Although some achievements have been made in slope stability analysis, the monitoring and early warning of instability have not been completely solved. The conventional monitoring adopts the 'point, line' layout, which has certain spatial limitations. In recent years, microseismic (MS) monitoring technology has been used as a high-precision

rock mass fracture and deformation safety monitoring method. By preembedding MS sensors in the monitoring target area, pick up the elastic waves released by microcrack inside the rock mass in real time, automatic inversion calculation quantitative seismic parameter, predict the macroscopic deformation and failure of the rock mass in advance, and then evaluate the overall stability of the engineering rock mass. Xu et al. [11, 12] successfully carried out MS monitoring of the high and steep rock slope on the left bank of Jinping first stage hydropower station and the right bank slope of Dagangshan hydropower station, evaluated the stability of the high rock slope of hydropower station, and achieved a lot of research results in the aspect of rock dynamic disaster.

The MS signal collected by the MS monitoring system is a complex nonlinear and nonstationary time series. The fracture of the slope rock mass often has the characteristics of discontinuous multiscale. Compared with the simple fractal dimension, the multifractal method can describe the fluctuation of the rock fracture signal at different levels more accurately. Multifractals, also known as multiscale fractals, represent self-similar fractal systems with different local characteristics. From the perspective of statistical physics, multifractal is an inhomogeneous set which consist of probability subsets with many different singular exponents. At present, the methods to estimate the multifractal spectrum mainly include box counting method, histogram method, partition function method, Wavelet-Based Detrended Fluctuation Analysis method (WB-DFA), Wavelet Transform Modulus Maxima method (WTMM), and Multifractal Detrended Fluctuation Analysis method (MF-DFA). The box counting method adopts a regular gridding method, which does not reflect the distribution of fractal body in the regional space, and the estimation of fractal dimension is very unstable in some cases [13]. The histogram method converges very slowly. Although the partition function method is relatively simple, its calculation results cannot fully reflect the distribution of singularity. Manimaran et al. [14] first proposed the WB-DFA method, which mainly used discrete wavelet transform to decompose signals and extract trends. It did not need to divide intervals in advance, and a certain shape of wavelet is used to approximate trends. However, when the data length is short and the spectrum is narrow, the calculation error is larger. WTMM was proposed by Mallat and Zhong [15], which mainly uses continuous wavelet transform for signal analysis, can process strong unsteady time series, and can estimate the local Hölder exponent, but it requires high-quality data and more detailed parameters to be adjusted and it cannot accurately distinguish between single fractal and multiple fractal. MF-DFA was first proposed by Kentelhardt et al. [16]. Compared with the previous method, its estimation result is better overall.

Based on the left bank slope of Baihetan hydropower station in Southwestern China, the MF-DFA method was adopted, the multifractal spectrum was estimated, the MF-DFA preset parameters were determined, the multifractal characteristics of the rock microcrack waveform and the blast vibration waveform were comparatively studied, and the nonlinear dynamic characteristics of the MS waveform were revealed. On this basis, the MS waveform multifractal time-varying response characteristics of rock slope deformation and failure process are discussed, and a rock slope deformation early warning model based on multifractal theory is established.

2. Engineering Background

2.1. Project Overview. The Baihetan hydropower station is located at the junction of Ningnan County in Sichuan Province and Qiaojia County in Yunnan Province, as shown in Figure 1. It is the second cascade hydropower station developed in the lower reach of Jinsha river. It is 182 km away from the upstream Wudongde hydropower station and 195 km away from the downstream Xiluodu hydropower station. The hydropower station adopts an all-underground powerhouse layout, and the left and right bank underground powerhouses adopt a symmetrical layout with a total installed capacity of 16000 MW. It is currently the second largest installed capacity hydropower station over the world. The excavation picture of slope excavation site is shown in Figure 2.

2.2. Geological Condition. The two sides of the dam site are syncline geology, and the river valley has an asymmetric 'V' shape with the left bank low and the right bank high. The typical section of the left bank slope along the dam arch axis is shown in Figure 3(a). The direction of the abutment on the left bank is approximately north-south and inclines 60° to the east. The stratum lithology of the left dam foundation is mainly composed of laminar basalt ($P_2\beta$) and a small amount of clastic rock (T_3x) and limestone (P_1m). The weak structural plane in the study area of the left bank slope mainly includes faults F14 and F17, interlayer staggered zones C3-1 and C3 developed along the rock strata, intraformational disturbed zones LS331 and LS337, and many structural cracks, as shown in Figure 3(a). The geological engineering plane figure of left bank slope is shown in Figure 3(b), and the strike rose diagram of dominant joints is shown in Figure 3(c) The mechanical properties of rock masses and weak structural planes were obtained by the experiment of Hydro-China Huadong Engineering Corporation, as shown in Table 1. The maximum principal stress is $\sigma 1 = 8.0$–11.0 MPa with orientation of N40W and dip angle of 15°, the medium principal stress is $\sigma 2 = 7.0$–9.0 MPa with orientation of N12E and dip angle of -48°, and the minimum principal stress is $\sigma 3 = 6.0$–8.0 MPa with orientation of N74E and dip angle of −29° [18].

3. MS Monitoring of the Left Bank Slope

The left bank slope of Baihetan hydropower station adopted the MS monitoring system produced by Canadian ESG (Engineering Seismology Group). The MS monitoring system was successfully installed and operated on November 10, 2014. The network topology of the MS monitoring system is shown in Figure 4. The MS monitoring network consists of a Hyperion data processing system, 3 Paladin data

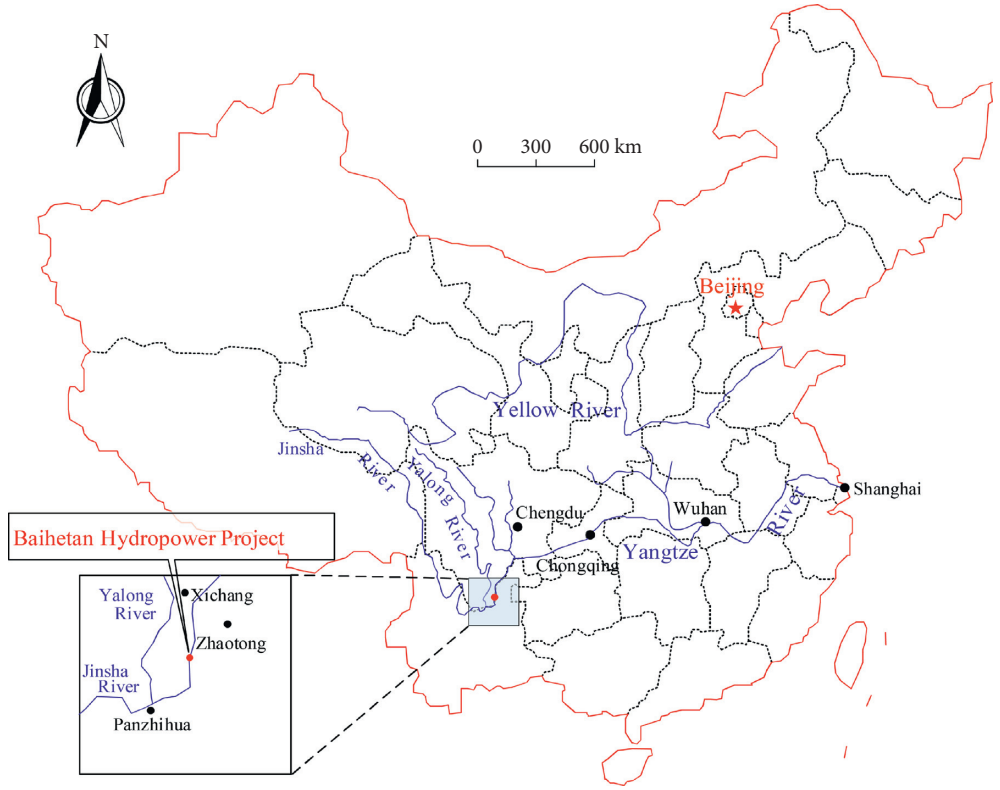

Figure 1: Geographical location of the Baihetan hydropower station [17].

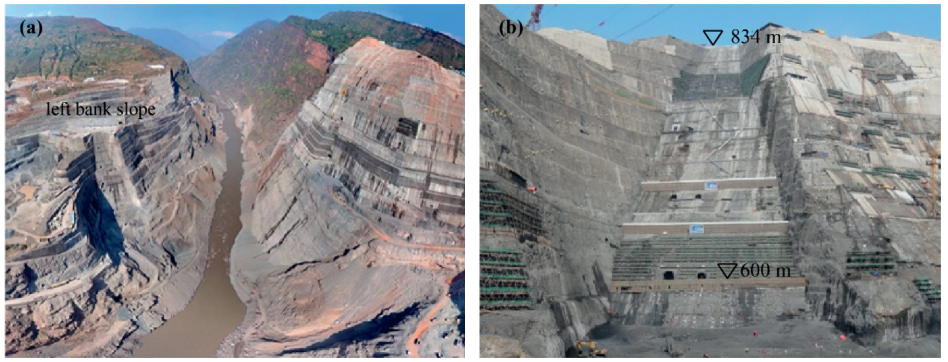

Figure 2: The pictures of slope excavation site: (a) full view of Baihetan hydropower station excavation; (b) the area of left bank slope spandrel groove.

acquisition substations, and 18 uniaxial acceleration sensors. The sensors are installed in the sidewalls of three tunnels (i.e., grouting tunnels and drainage tunnels) at different elevations (i.e., 610 m, 660 m, and 750 m). Hyperion data processing system mainly includes HANS signal real-time acquisition and recording software, WaveVis waveform processing software, and SeisVis 3-dimensional visualization software. The HANS signal real-time acquisition and recording software can control parameters such as the sampling frequency, signal gain, and signal trigger threshold of Paladin data acquisition substation. The sampling frequency of the MS monitoring system in the left bank slope of Baihetan is 20 kHz, the threshold value of the ratio of short to long Windows is adopted to trigger, with a threshold value of 3, and the response frequency range of the sensor is 50 Hz~5 kHz. WaveVis waveform processing and analysis software can automatically identify or manually process the collected waveform files and obtain the time, position, moment magnitude, energy release, and other parameters of MS events through inversion calculation. The SeisVis 3-dimensional visualization software can display the processing results of MS events in real time and identify the potential danger areas by analyzing the activity characteristics of MS events. The sensor receives the elastic wave to generate an electrical signal, which is transmitted to Paladin substation via the cable. Paladin data acquisition substations transmit the collected MS data to Hyperion processing system through communication cable (optical fiber cable).

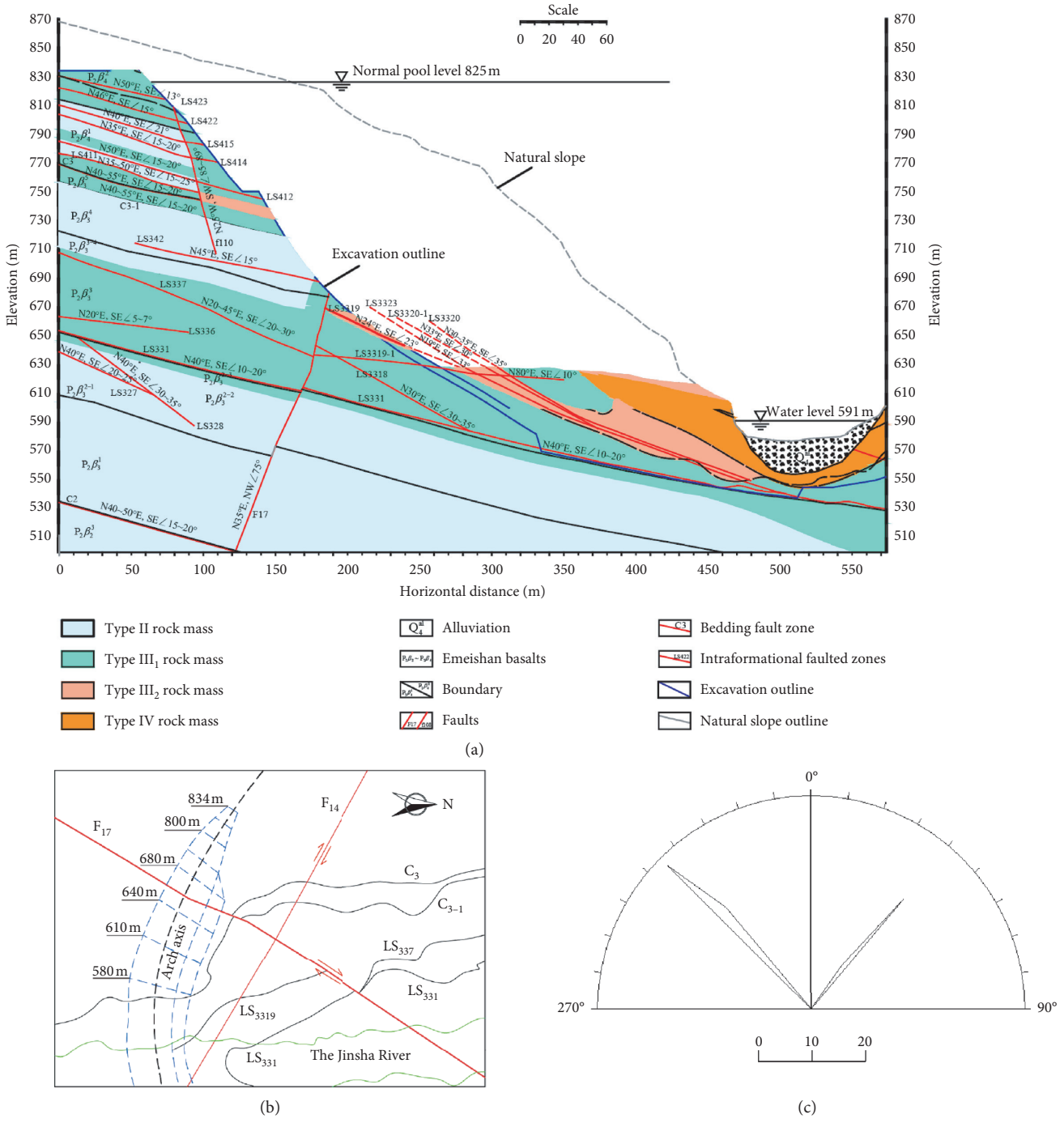

Figure 3: Arch axis geological section of the left bank slope, (a) geological engineering plane figure of left bank slope, (b) and the strike rose diagram of dominant joints (c) [17].

Hyperion data processing system automatically filters background noise and completes record storage of MS events, providing users with complete waveform and spectrum information for analysis and research.

With comprehensive consideration of economic conditions, technical conditions, and engineering conditions, aiming at the problems of excavation deformation and safety construction of the left bank slope of Baihetan hydropower station, the optimal arrangement plan of sensors of the MS monitoring system is proposed as shown in Figure 5.

4. Multifractal Detrended Fluctuation Analysis

4.1. Basic Principle of the MF-DFA Method. Fractal is generally divided into two categories, one is geometric self-similarity or uniform fractal, and the other is statistical self-similarity or nonuniform fractal, i.e., multifractal. Geometric

Table 1: Mechanical properties of the main rock masses and weak structural planes.

Rock mass type	Compressive strength (MPa)	Elasticity modulus (GPa)	Poisson's ratio	Density (g/cm^3)	Shear strength /(°)	Shear strength c (MPa)
II	100	15	0.23	2.80	36	1.4
III1	70	12	0.24	2.68	36	1.1
III2	55	11	0.26	2.60	35	0.75
IV	35	5	0.32	2.50	33	0.5
F17	23	1	0.34	2.13	28	0.15
C3-1	22	0.71	0.35	2.05	28	0.04
C3	18	0.4	0.34	2.13	28	0.1
LS331	23	1.3	0.35	2.15	27	0.06
LS337	18	0.2	0.35	2.03	25	0.05

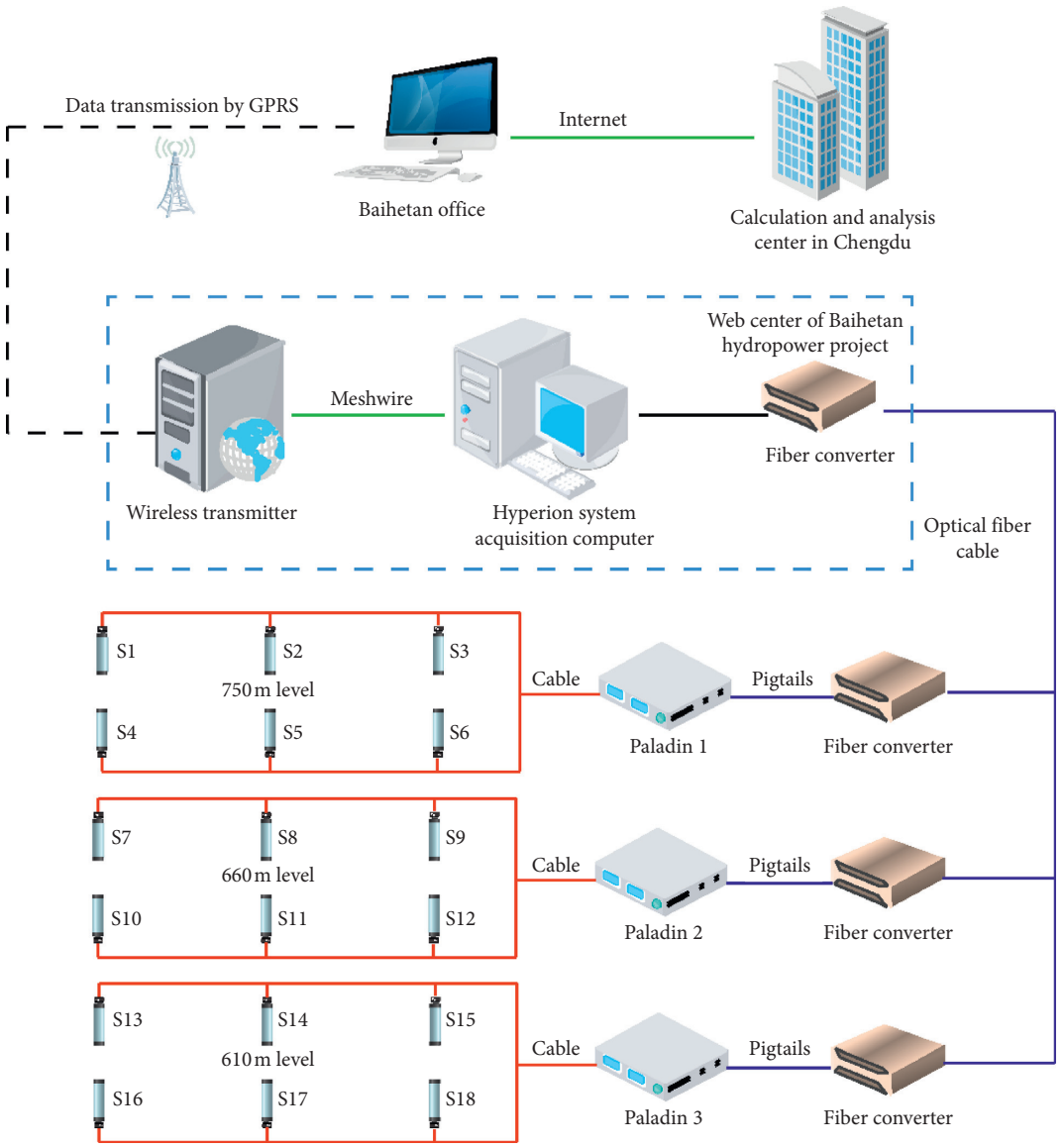

Figure 4: Network topology of the MS monitoring system.

self-similarity is usually described by a simple fractal dimension D, but the fractal in nature is generally statistically self-similar, which needs to be described by the multifractal spectrum $f(\alpha) - \alpha$. Multifractal spectrum $f(\alpha) - \alpha$, also known as singular spectrum, is a commonly used parameter to describe multifractal. The segmented structure of singular measure can be analyzed by multifractal spectrum [19]. In multifractal calculation, the fractal body will be divided into

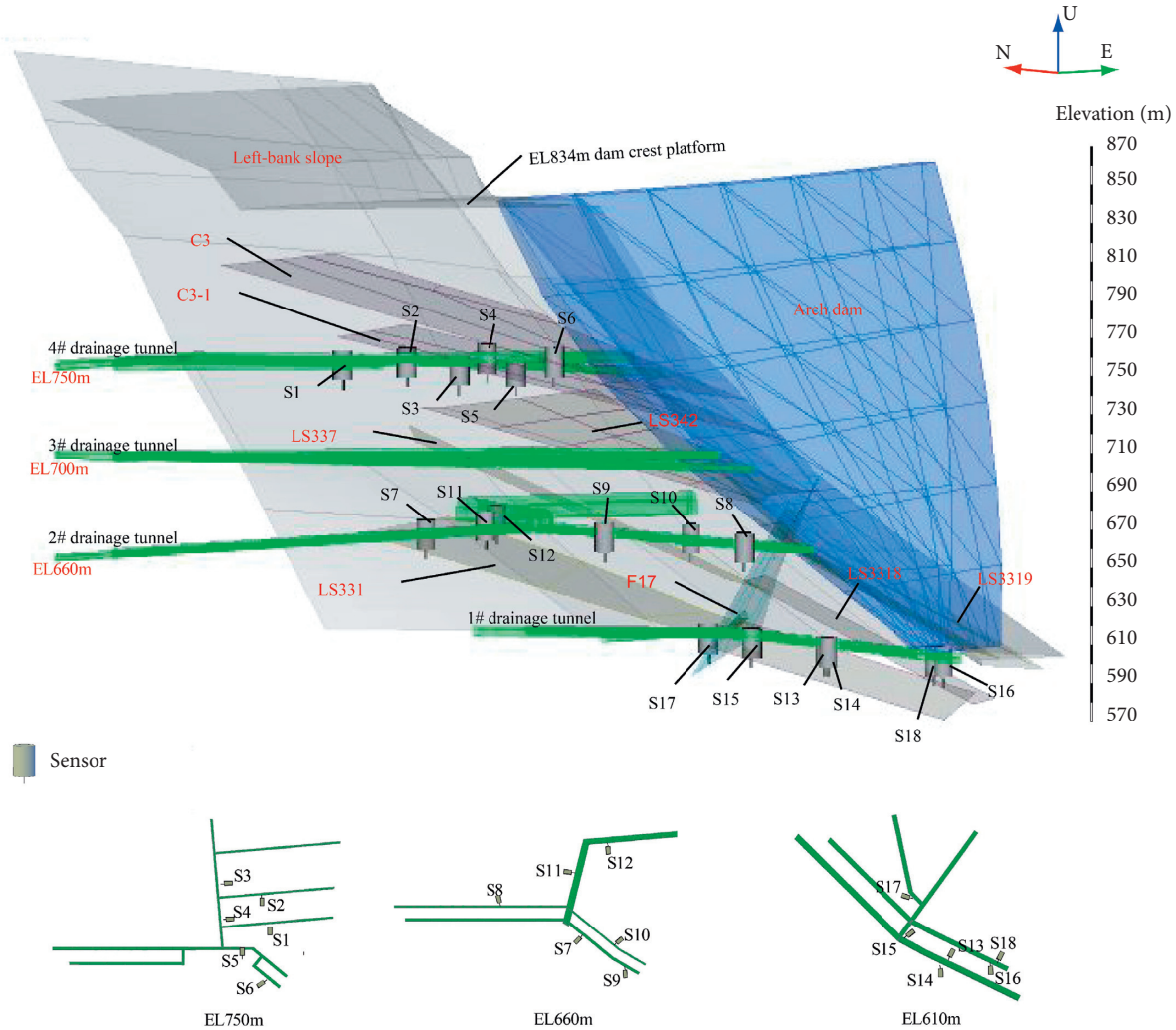

Figure 5: Spatial arrangement diagram of the sensor in the left bank slope.

multiple intervals. Among them, α is the singularity exponent, which represents the fractal dimension of a certain interval, the fractal dimension of each interval can be expressed by the corresponding α, and the intervals with the same α value form a fractal subset. Due to the large number of intervals, a multifractal spectrum function $f(\alpha)$ composed of infinite sequences of different α can be obtained.

Multifractal Detrended Fluctuation Analysis (MF-DFA) is an extension of Detrended Fluctuation Analysis (DFA), which can effectively reveal the dynamic behavior in nonlinear and nonstationary signals. Compared with the traditional multifractal calculation method, the core advantages of MF-DFA mainly have three points: (1) make full use of the sequence data length and divide the sequence into equal time length in forward and reverse; (2) fitting polynomials are for each interval by least squares to eliminate the impact of nonstationary trends in time series; (3) analyze the behavior of time series at different levels by using volatility functions of different orders and accurately describe the fractal characteristics of time series, revealing the multifractal characteristics hidden in nonstationary time series.

4.2. Algorithm of the MF-DFA Method. The MF-DFA calculation program consists of five steps, of which the first three steps are traditional DFA.

Let the time series of the MS waveform signal be $\{x(k), \quad k = 1, 2, \ldots, N\}$, which is a nonlinear and nonstationary sequence.

Step 1: construct the signal profile:

$$Y(i) = \sum_{k=1}^{i} [x_k - \langle x \rangle], \quad i = 1, 2, \ldots, N, \tag{1}$$

where $\langle x \rangle$ is the mean of the time series $\{x(k)\}$; i.e.,

$$\langle x \rangle = \frac{1}{N} \sum_{k=1}^{N} x_k. \tag{2}$$

Step 2: divide the signal profile $Y(i)$ into N_s intervals of equal time length s; i.e.,

$$N_s = \text{int}\left(\frac{N}{s}\right). \tag{3}$$

Since N is not necessarily an integer multiple of s, the signal profile $Y(i)$ will have a residual value during the division process. In order to make full use of the data and retain this part of the residual value, the above division process can be repeated from the tail of the signal profile $Y(i)$; at this time, $2N_s$ equal length intervals will be obtained.

Step 3: the least square method is used to fit the local trend of the data in each interval in Step 2, and then the variance is calculated. This step is the most time-consuming part of the MF-DFA.

When $v = 1, 2, \cdots, N_s$,

$$F^2(s, v) = \frac{1}{s}\sum_{i=1}^{s}\left\{Y\left[(v-1)s + i\right] - y_v(i)\right\}^2. \tag{4}$$

When $v = N_s + 1, N_s + 2, \ldots, 2N_s$,

$$F^2(s, v) = \frac{1}{s}\sum_{i=1}^{s}\left\{Y\left[N - (v - N_s)s + i\right] - y_v(i)\right\}^2. \tag{5}$$

where $y_v(i)$ represents the m-order ($m = 1, 2, 3, \ldots$) fitting polynomial in vth interval.

In the time series, the elimination of the 'trend' is completed by subtracting the fitting polynomial $y_v(i)$ from the signal profile $Y(i)$, so different fitting orders m can reflect the degree of elimination of 'trend.'

Steps 1–3 are the traditional DFA method.

Step 4: calculate q-order volatility function $F_q(s)$:

$$F_q(s) = \left\{\frac{1}{2N_s}\sum_{v=1}^{2N_s}\left[F^2(s, v)\right]^{q/2}\right\}^{1/q}. \tag{6}$$

When $q = 2$, MF-DFA degenerates into standard DFA.

Step 5: make q-order volatility function $F_q(s) - s$ double logarithmic graph.

If $\{x(k)\}$ has self-similarity characteristics, i.e., $\{x(k)\}$ is a multifractal time series, then there is a power law relationship between q-order volatility function $F_q(s)$ and s:

$$F_q(s) \sim s^{h(q)}, \tag{7}$$

where $h(q)$ is the generalized *Hurst* exponent, which represents the correlation of the original sequence and the size of $h(q)$ depends on the value of q. For stationary time series, when $q = 2$, $h(2)$ is the same as *Hurst* exponent. Normally, $F_q(s)$ is an increasing function of s.

If $\{x(k)\}$ is a single fractal time series, $F^2(s, v)$ has the same scale among all intervals, and $h(q)$ is a constant, independent of the value of q.

In particular, when $q = 0$, formula (6) diverges, and then $h(0)$ can be determined by the logarithmic averaging process:

$$F_0(s) \equiv \exp\left\{\frac{1}{4N}\sum_{v=1}^{2N_s}\ln\left[F^2(v, s)\right]\right\} \approx s^{h_0}. \tag{8}$$

4.3. Estimation of the Standard Multifractal Spectrum by the MF-DFA Method. The generalized *Hurst* exponent $h(q)$ obtained in the previous section is closely related to the mass exponent $\tau(q)$ based on the partition method.

Now suppose that the time series $\{x(j), j = 1, 2, \ldots, N\}$ is a stable and normalized time series. $\{x(j)\}$ does not need to eliminate the "trend." Detrended Fluctuation Analysis (DFA) can be simplified and replaced by Fluctuation Analysis (FA). Formula (4) can be rewritten as

$$F_{FA}^2(s, v) \equiv \left[Y(vs) - Y((v-1)s)\right]^2. \tag{9}$$

Substitute $F_{FA}^2(s, v)$into formulas (6) and (7) and get

$$\left\{\frac{1}{2N_s}\sum_{v=1}^{2N_s}\left|Y(vs) - Y((v-1)s)\right|^q\right\}^{1/q} \sim s^{h(q)}. \tag{10}$$

For simplicity, assume that the length of $\{x(j)\}$ is an integer multiple of equal time length s; i.e.,

$$N_s = \frac{N}{s},$$
$$\sum_{v=1}^{N/s}\left|Y(vs) - Y((v-1)s)\right|^q \sim s^{qh(q)-1}. \tag{11}$$

According to the definition of profile $Y(i)$ constructed in formula (1), the box probability measure $P_s(v)$ can be obtained:

$$P_s(v) \equiv \sum_{j=(v-1)s}^{vs} x_j = Y(vs) - Y((v-1))s). \tag{12}$$

The mass exponent $\tau(q)$ is determined by the partition function $\chi_q(s)$:

$$\chi_q(s) = \sum_{v=1}^{N/s}\left|P_s(v)\right|^q \sim s^{\tau(q)}. \tag{13}$$

By comparing formulas (12) and (13), the following can be obtained:

$$\tau(q) = qh(q) - 1. \tag{14}$$

The generalized multifractal dimension $D(q)$ can be expressed as

$$D(q) = \frac{\tau(q)}{q-1} = \frac{qh(q) - 1}{q-1}. \tag{15}$$

It is worth noting that, as mentioned in the previous section, for a single fractal time series, $h(q)$ has nothing to do with the value of q, but the generalized multifractal dimension $D(q)$ is still related to the value of q.

The singularity exponent α and the multifractal spectral function $f(\alpha)$ can be obtained through the change of Legendre:

$$\begin{aligned} \alpha &= \tau'(q) = \alpha = h(q) + qh'(q), \\ f(\alpha) &= q\alpha - \tau(q) = q[\alpha - h(q)] + 1. \end{aligned} \tag{16}$$

According to the above algorithm, the calculation process is shown in Figure 6.

4.4. Key Parameter Setting of the MF-DFA Method. Multifractal theory has been widely applied in many fields such as physics, biomedicine, economics, materials science, and geology [20]. The characteristics of the nonstationary time series obtained under different conditions are obviously different, such as the length of the signal time window and the fluctuation trend. Therefore, it is necessary to trial calculation and preset the key parameters to obtain more reliable estimation results. Key parameters of multifractal mainly include time length s, weight factor q, and fitting order m. The value of the parameter affects the calculation result from different aspects, and, at the same time, we can understand the application of multifractal theory in engineering MS monitoring from a deeper level. The parameters of the MS waveform of the left bank slope of Baihetan are calculated and preset as follows.

4.4.1. Time Length s. In the calculation program, the divided time length s is used to calculate the local fluctuation root mean square (RMS). Before determining the length of time s, there are two important premises: (1) the minimum time length s ($s_{\min}$) must be much larger than the polynomial fitting order m, to prevent the overfitting of the polynomial trend and to prevent the fitting trend from being similar to the time series and making the residual fluctuation close to 0. (2) The maximum length of time s ($s_{\max}$) should make the number of intervals involved in the calculation larger than 10 [21]. Since the time series $\{x(k)\}$ in MF-DFA algorithm is divided by equal time length in both directions, the number of sampling points should be at least 5 times of the time length $s_{\max}$.

Taking the time series of the MS event waveform in the left bank slope of Baihetan at 13 : 30 on June 15, 2016, as an example, q-order volatility function $F_q(s) - s$ double logarithmic graph is shown in Figure 7(a) where the fitting order $m = 3$ and the different color curves represent $F_q(s) - s$ double logarithmic relationship corresponding to different q values. The value of q ranges from −20 to 20, the equal component $\Delta q = 0.04$, and a total of 101 curves were obtained. According to formula (7), the slope of the fitting curve is generalized *Hurst* exponent, which is used for the estimation of multifractal spectrum, as shown in Figure 7(b). It can be clearly seen from Figure 7 that when $\mathrm{Log}_2(s) =$ 8~12, the fitting effect is better. In particular, the local *Hurst* exponent $h(q)$ with a large time length will show a smooth and slow change trend, which is related to a large calculation interval and a small number of intervals.

Based on the above considerations, the value of the multifractal time length s of the MS signal in the left bank slope of Baihetan is $s_{\min} = 2^8 = 256$ and $s_{\max} = 2^{12} = 4096$.

4.4.2. Weight Factor q. The value of the weight factor q should include positive and negative values in order to periodically weight the fluctuation changes in the time series. The size of q value represents the proportion of the RMS of local fluctuations in the whole. For a large q value, it means that the big fluctuation occupies the dominant position in the whole time series. $h(q)$ mainly describes the scale behavior of the big fluctuation. On the contrary, for small q value, small fluctuations are dominant, and $h(q)$ mainly describes the scale behavior of small fluctuations. Therefore, the value of q should avoid larger or smaller values to reduce the error they caused at the tail of the multifractal spectrum. In the actual calculation, when the value of q has no significant effect on the calculation result, the range of value of q can be cut off [22].

Four typical MS event waveform time series in the left bank slope of Baihetan were selected for MF-DFA calculation. The absolute value of q ranged from 0.5 to 50. The calculation results are shown in Table 2. It can be clearly seen from Table 2 that when $|q|$ was 0.5~20, the value of $\Delta\alpha$ varies greatly, indicating that the value of q has a great effect on the calculation result. Therefore, the value range of q should be increased. However, when $|q|$ was 20~50, the variation error was controlled within 0.01, indicating that when $|q|$ was 20, the calculation result has tended to be stable, and the range of q can be cut off.

The same result can also be obtained from $h(q) - q$ graph shown in Figure 8. The values of $|q|$ are 0.5, 3, 20, and 50, respectively. When $|q|$ was 0.5, $h(q) - q$ graph was approximately a straight line; when $|q|$ was 3, $h(q) - q$ graph had a certain curvature; and when q was 20 and 50, two curves had a certain similarity. From the perspective of 'global-local,' $h(q) - q$ graph when $|q|$ was 0.5 and 3 can be regarded as the 'local distribution graph' of the central part of $h(q) - q$ when $|q|$ was 20 and 50. Therefore, it cannot fully reflect the overall trend of $h(q) - q$ graph.

4.4.3. Fitting Order m. In the MF-DFA calculation, the larger fitting order m can ensure that the multifractal spectrum is not affected by the nonstationary trend in the time series. However, a larger value of m may lead to overfitting of a small sample time series, and the calculation time will increase. In the calculation process, in order to ensure the stability of $F_q(s)$, m should also satisfy $m + 2 \le s$ [23].

Taking the waveform of the MS event in the left bank slope of Baihetan at 13 : 30 on June 15, 2016, as an example, $Fq(s) - s$ relationships at different m orders are calculated, respectively, and the contour projection is shown in Figure 9. It can be seen from Figure 9 that when $m = 1$~2, $Fq(s) - s$ relationship fluctuates greatly and the fitting effect is not good, while when $m \ge 3$, the fitting effect is better.

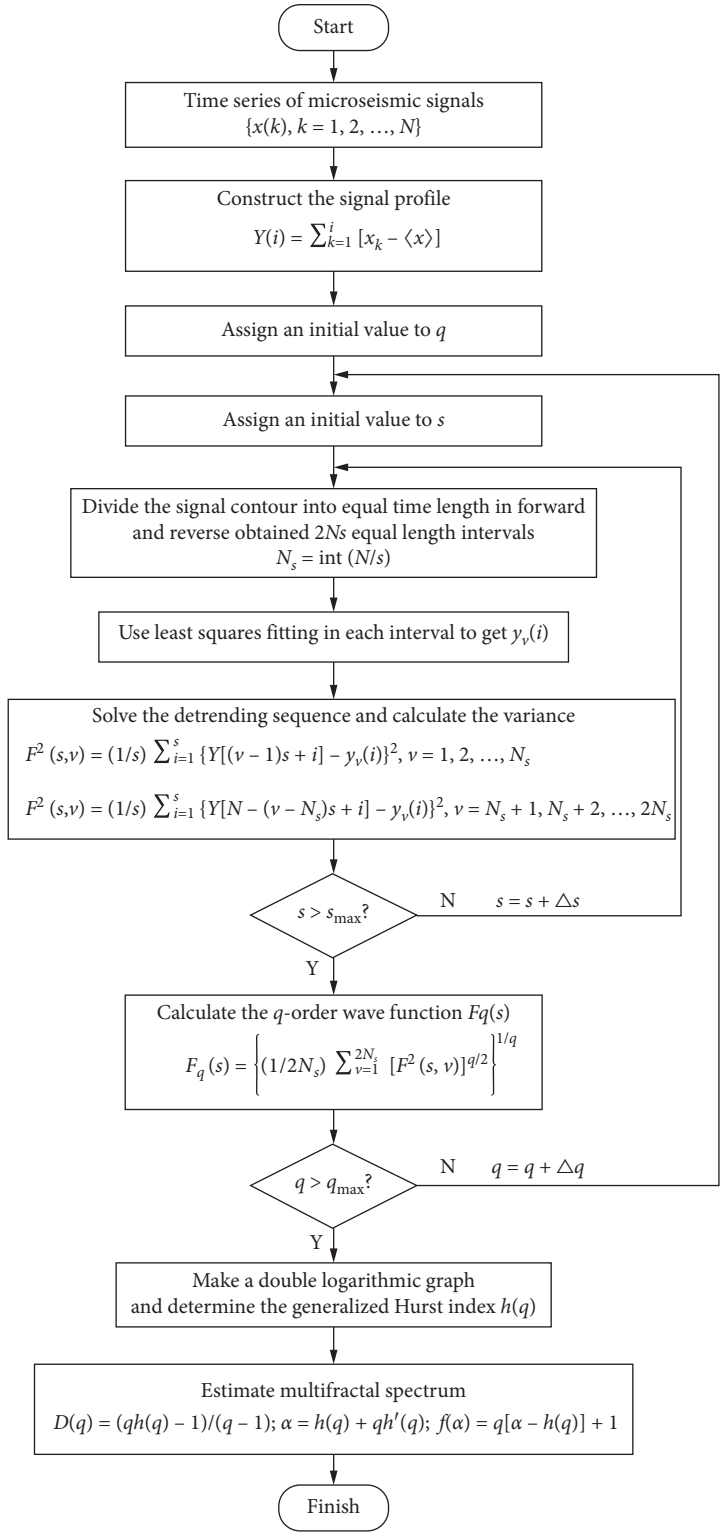

Figure 6: MF-DFA calculation flow chart.

Considering the huge amount of data and the calculation time, the fitting order in the multifractal calculation of the MS waveform on the left bank slope of Baihetan is $m = 3$.

In summary, the preset parameters of MS multifractal of the left bank slope of Baihetan hydropower station are as follows:

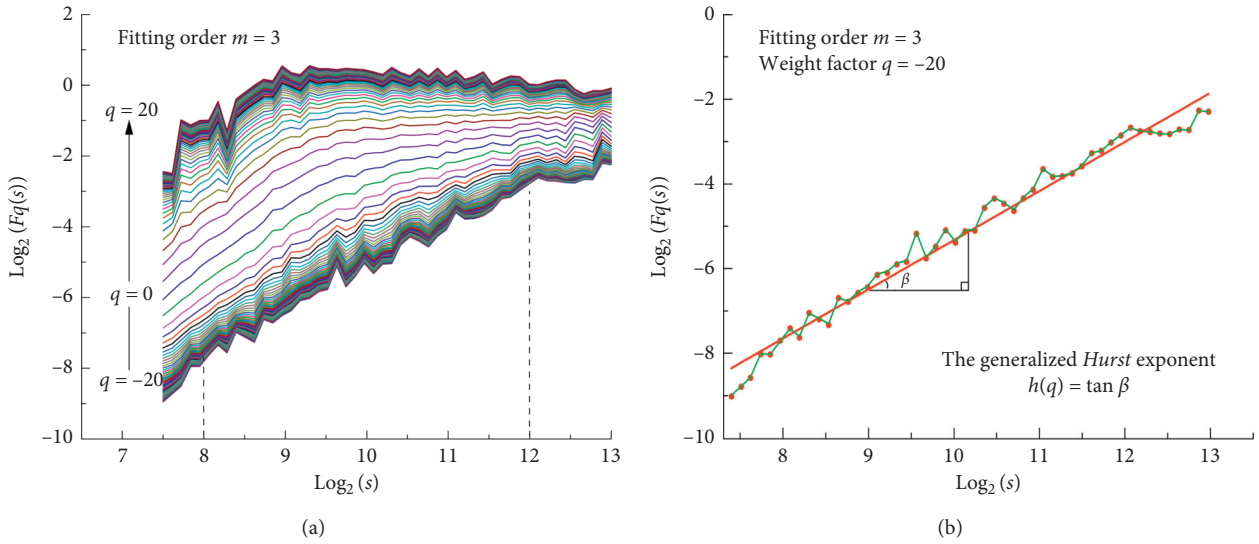

Figure 7: Determining the length of time s: (a) $F_q(s) - s$ double logarithmic graph; (b) generalized Hurst exponent.

Table 2: Calculation of the width of the multifractal spectrum $\Delta\alpha$.

Time of MS event	Weight factor $\lvert q\rvert$							
	0.5	1	3	5	10	20	30	50
06–30 02 : 46 : 24	0.3302	0.5070	0.5938	0.6686	0.7614	0.7991	0.8052	0.8075
06–24 15 : 50 : 31	0.3697	0.5300	0.6600	0.7318	0.8217	0.8521	0.8568	0.8591
06–18 04 : 37 : 29	0.0907	0.1872	0.4248	0.5325	0.6241	0.6524	0.6555	0.6566
06–15 13 : 30 : 01	0.4121	0.6721	0.8987	0.9927	1.0679	1.0890	1.0920	1.0930

Note. The calculation result retains four decimal places.

$$\begin{aligned} s_{\min} &= 2^8 = 256, \\ s_{\max} &= 2^{12} = 4096, \\ |q| &= 20, \\ m &= 3. \end{aligned} \tag{17}$$

5. Multifractal Characteristics of MS Signals

The signals collected by MS monitoring of rock slope mainly include rock microfracture signals (MS signals), blasting vibration signals (blasting), mechanical vibration signals, current interference signals, car whistle, and unknown signals. The multifractal characteristics of different signals are obviously different. The following mainly analyzes the multifractal characteristics of rock microfracture and blasting vibration waveform time series by MF-DFA method.

5.1. Multifractal Spectrum of MS Signals. Figure 10 shows the typical rock microfracture signal and rock blasting vibration signal, and Figure 11 shows the multifractal spectrum corresponding to the two types of typical signals.

In Figure 11, $\Delta\alpha$ is the width of the multifractal spectrum, which represents the multifractal strength of the waveform and the complexity of the fluctuation. The larger the $\Delta\alpha$ is, the greater the multifractal strength of the waveform is, and the more intense and complex the fluctuation is. And vice versa, the calculation can be expressed as $\Delta\alpha = \alpha_{\max} - \alpha_{\min}$. It can be seen from Figure 11 that the multifractal spectrum width of rock microfracture waveform $\Delta\alpha_1 = 0.99$ is much smaller than the multifractal spectrum width of blasting vibration waveform $\Delta\alpha_2 = 3.14$, indicating that the multifractal strength of blasting vibration waveform is larger and the fluctuation is more intense and complex. $\Delta f(\alpha)$ represents the proportion of large fluctuations and small fluctuations in the waveform. The larger the $\Delta f(\alpha)$ is, the larger the proportion of small fluctuations in the waveform will be and vice versa. The calculation can be expressed as $\Delta f(\alpha) = f(\alpha_{\max}) - f(\alpha_{\min})$. It can be seen from Figure 11 that the multifractal spectrum of rock microfracture waveform $\Delta f(\alpha_1) = -0.06$, which is larger than the multifractal spectrum of blasting $\Delta f(\alpha_2) = -0.21$, indicating that small fluctuations in the MS waveform account for a large proportion.

5.2. Multifractal Characteristics of Rock Microfracture Waveform with Background Noise. In the previous section, the multifractal characteristic of a typical MS waveforms is described. However, in actual MS monitoring of rock slope, the collected MS signals were often mixed with various types of noise due to the complexity of the engineering field construction and the rock mass itself. The following studied the effect of background noise on multifractal spectrum estimation by MF-DFA calculation.

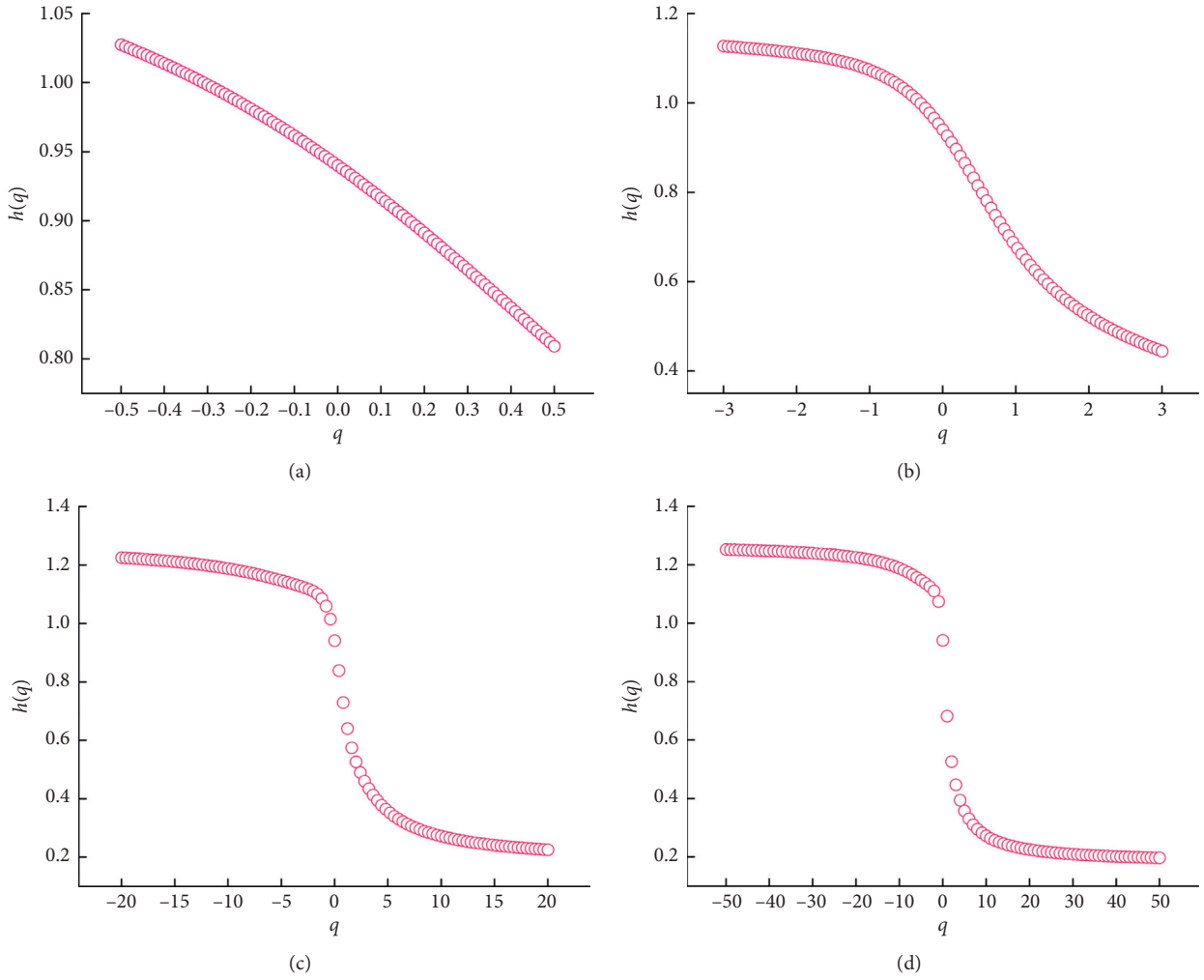

Figure 8: Determining the weight factor q: (a) $q\in[-0.5, 0.5]$, (b) $q\in[-3, 3]$, (c) $q\in[-20, 20]$, and (d) $q\in[-50, 50]$.

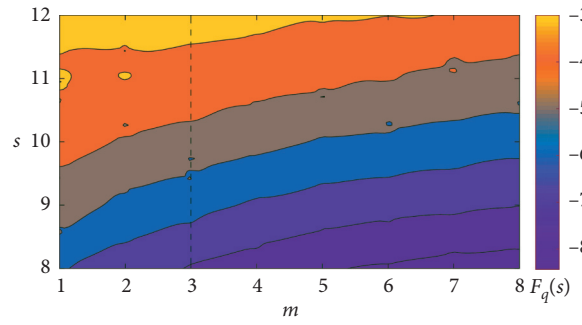

Figure 9: Different m-order $F_q(s) - s$ relationship contour projection.

The MS waveforms $A\sim J$ with background noise collected by different channels at the same time were selected for MF-DFA calculation, and the waveform is shown in Figure 12. It can be seen from Figure 12 that the amplitudes of the waveforms from $A\sim J$ are in descending order, including ADHJ with a large background noise and BCEF with a small background noise. The mass exponent $\tau(q) - q$ graph and the multifractal spectrum $f(\alpha - \alpha)$ graph were made for $A\sim J$, as shown in Figure 13. Figures 13(a) and 13(b) show the multifractal characteristics of waveform corresponding to the window size of 1500 ms, and Figures 13(c) and 13(d) show the multifractal characteristics of the waveform corresponding to the window size of 750 ms (i.e., 375 ms to 1125 ms in Figure 12). There are two main advantages of focusing the multifractal analysis window on the effective waveform area: (1) speeding up calculation efficiency,

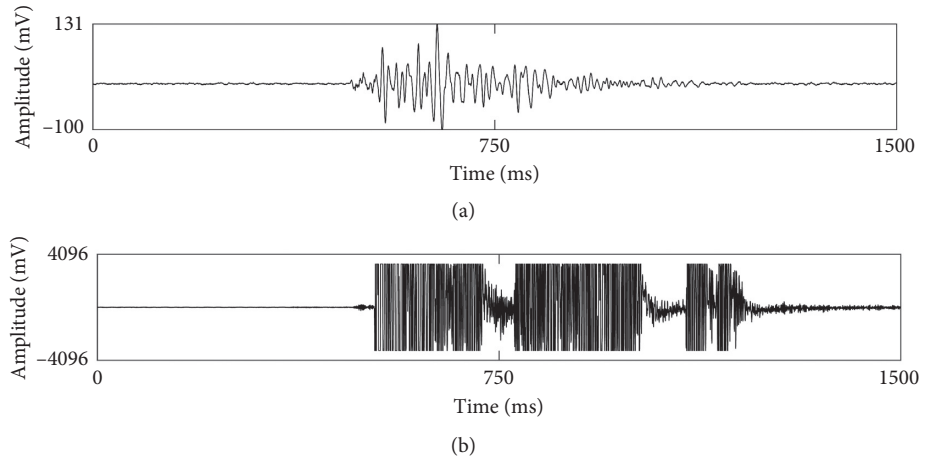

Figure 10: Typical signal waveform: (a) rock microfracture signals; (b) blasting vibration signals.

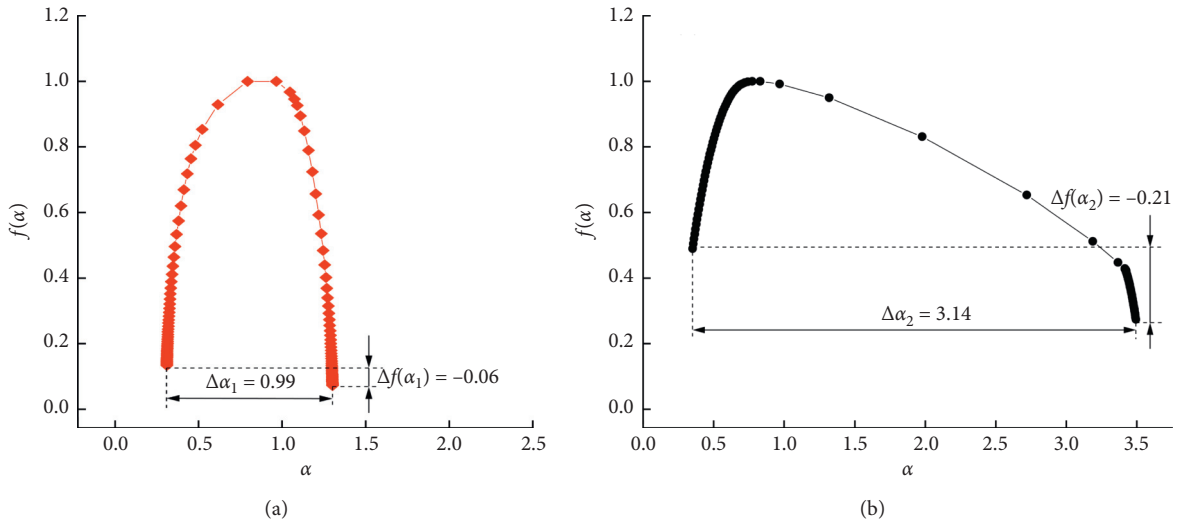

Figure 11: Multifractal spectrum of typical signal: (a) MS signal; (b) blasting signal.

suitable for a large number of waveform multifractal calculations, and (2) better reflecting the multifractal characteristics of effective waveforms, which is beneficial to distinguish the multifractal difference of waveform produced by different inducements. In general, different waveforms for multifractal difference analysis should ensure the same time window size.

According to the mass exponent $\tau(q) - q$ graph shown in Figure 13(a), the curve corresponding to the rock microfracture waveform ADHJ with background noise is located above the left end and below the right end in the mass exponent $\tau(q) - q$ graph. Meanwhile, the waveform ADHJ has a smaller $\alpha_{\max}$ in the multifractal spectrum $f(\alpha) - \alpha$ diagram shown in Figure 13(b). The time window was narrowed to make the rock microfracture waveform fill the window as much as possible, to improve the effectiveness of waveform multifractal analysis, and MF-DFA was calculated again. The results of the recalculation are shown in Figures 13(c) and 13(d). The calculation results are more obvious: the width of the multifractal spectrum $\Delta\alpha$ of the rock microfracture waveform ADHJ with large background noise is small, and the microfracture waveform BC with low background noise and large amplitude has a larger spectrum width $\Delta\alpha$.

This result reflects the effectiveness of MF-DFA method in removing nonstationary trend; that is, MF-DFA method puts more emphasis on the multifractal characteristics of rock microfracture waveform after removing noise. Therefore, when the MF-DFA is used to analyze the MS waveform data collected at different channels without sufficient noise filtering, the waveform with small background noise and large amplitude should be selected for analysis as much as possible to improve the reliability of multifractal spectrum estimation.

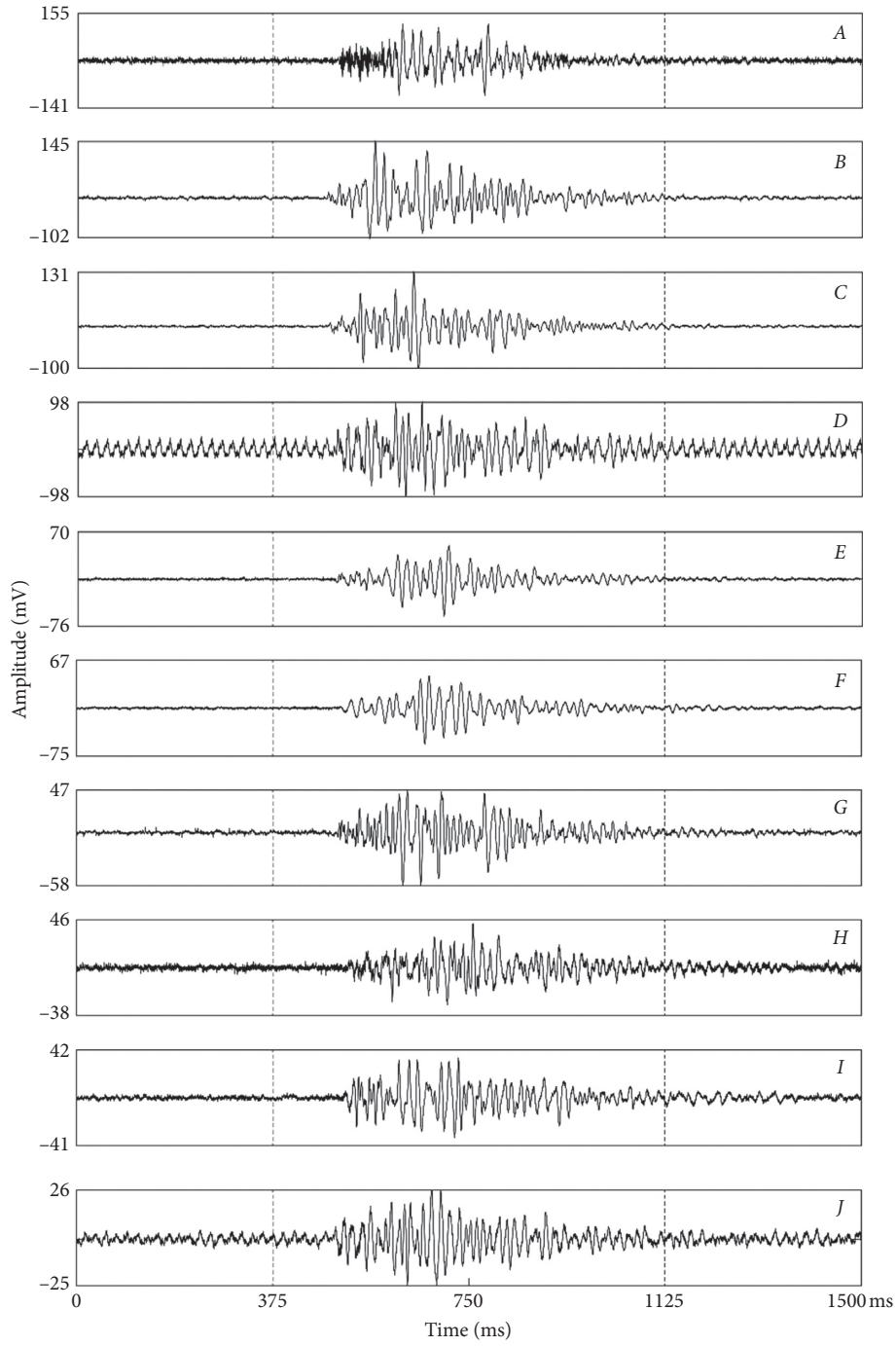

Figure 12: MS waveforms with background noises.

6. Multifractal Time-Varying Response Characteristics of MS Waveform and Deformation Warning of Rock Slope

6.1. Multifractal Time-Varying Response Characteristics of MS Waveform. Multifractal analysis was conducted on the MS waveforms of the rock mass near the crack T3301 (rock mass within 570 m~630 m elevation) of the left bank slope of Baihetan on June 1 to July 10, 2016. The crack T3301 is shown in Figure 14. The multifractal spectrum parameter $\Delta\alpha$ reflects the multifractal strength and the degree of fluctuation of the waveform time series, while $\Delta f(\alpha)$ reflects the proportion of large and small fluctuations in the waveform time series. The multifractal spectrum parameters $\Delta\alpha$ and $\Delta f(\alpha)$ represent the multifractal characteristics of the time series of rock microfracture waveform. The deformation and instability failure of rock slope is caused by the initiation, development, expansion, interaction, and connection of microfractures in rock mass, which is a nonstationary dynamic evolution process in time series. Therefore, it is

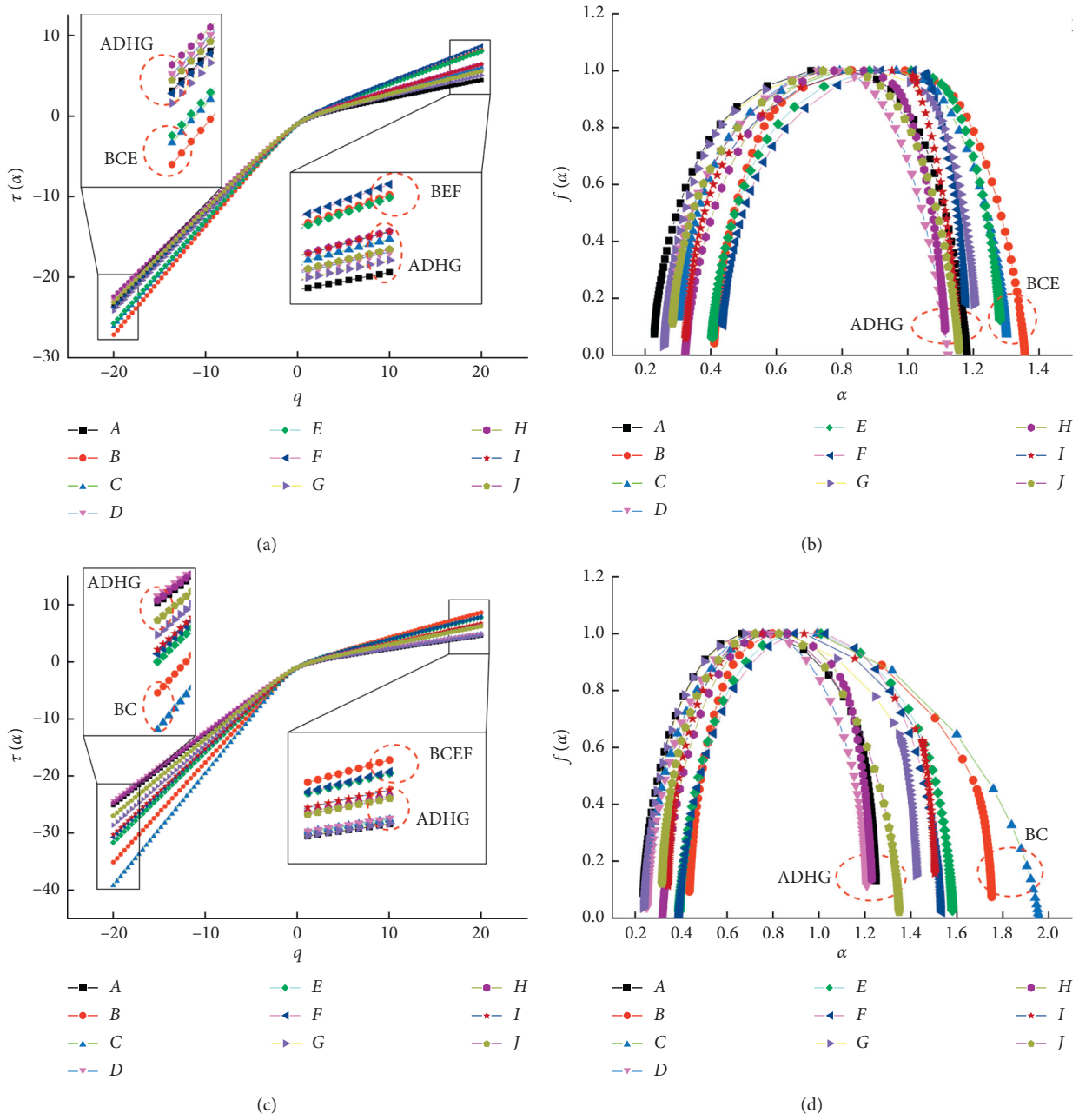

Figure 13: Multifractal characteristics of MS waveform with background noise: (a) $\tau(q) - q$ graph with window size of 1500 ms; (b) $f(\alpha) - \alpha$ graph with window size of 1500 ms; (c) $\tau(q) - q$ graph with window size of 750 ms; (d) $f(\alpha) - \alpha$ graph with window size of 750 ms.

necessary to focus on the analysis of the time-varying multifractal characteristics of the rock microfracture waveform during the monitoring period. Combined with the field macrofailure law, a rock slope deformation early warning model based on the MS waveform multifractal time-varying response characteristics was established.

Figure 15 shows the time-varying law of multifractal spectrum parameters $\Delta\alpha$ and $\Delta f(\alpha)$ of the MS waveform of the rock mass near the crack T3301. In Figure 15, the upper limit of $\Delta\alpha$ and the lower limit of $\Delta f(\alpha)$ have very obvious time series characteristics, so the evolutionary trend of $\Delta\alpha$ takes the upper limit of the MS event, and the evolutionary trend of $\Delta f(\alpha)$ takes the lower limit. As can be seen from Figure 15, since June 1, the number of MS events had not increased rapidly, but the overall $\Delta\alpha$ showed a sharp increase trend, reaching a maximum of 1.53, indicating that the multifractal strength of rock microfracture waveform increased and the fluctuations became complex and intense. The corresponding $\Delta f(\alpha)$ showed a sharp decrease trend; the minimum reached −0.58, indicating that the proportion of large fluctuations in the waveform time series increased. This was due to the strong unloading effect of blasting excavation, which hinders the further expansion of microcracks in hard rock mass. The number of MS events induced was small, but

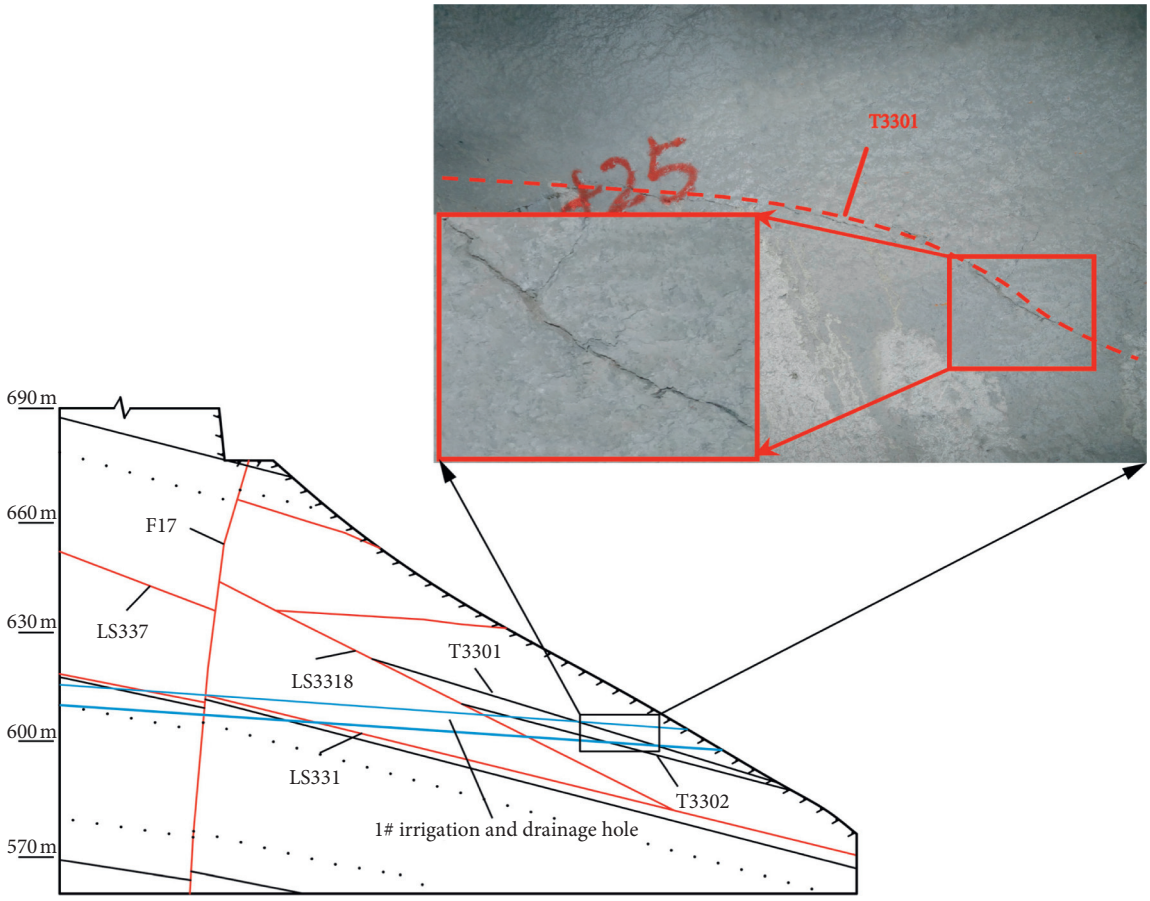

Figure 14: The location and photograph of T3301 crack.

the local stress was highly concentrated and the strain energy was increased, that is, the 'quiet period' before deformation and failure [24]. After June 15, $\Delta\alpha$ briefly fell back to the valley and then increased to 1.3 again and the corresponding $\Delta f(\alpha)$ increased from the valley. In this process, the local stress continued to increase until the rock bearing capacity was exceeded, resulting in the connection of microcracks at some locations, the stress concentration position began to shift, and the strain energy began to be released. When the crack expansion was blocked again, the local stress reconcentrated, and the strain energy accumulated again. After June 29, $\Delta\alpha$ decreased as a whole and was in a stable state, indicating that the fluctuation of the microfracture waveform time series was relatively smooth. And the value of $\Delta f(\alpha)$ also stabilizes near the zero line after a small increase. At this time, the microcracks almost were completely connected under the action of high stress, forming cracks, causing macroscopic failure, and the stress and strain energy were released.

6.2. Comparison with Conventional Monitoring. The time-varying response characteristics of multifractal spectrum parameters $\Delta\alpha$ and $\Delta f(\alpha)$ were closely related to the initiation, development, expansion, and penetration of rock microfractures. Before the deformation and failure of the rock mass, $\Delta\alpha$ showed an increasing trend and $\Delta f(\alpha)$ showed a decreasing trend, which can be regarded as a precursor signal of deformation warning; when deformation and failure occurred, $\Delta\alpha$ showed a decreasing trend and $\Delta f(\alpha)$ showed an increasing trend, which can be regarded as a deformation failure period; after deformation and failure, both $\Delta\alpha$ and $\Delta f(\alpha)$ showed a steady trend, and $\Delta f(\alpha)$ as a whole would be near the zero line, which can be regarded as a stable period. The division result is shown in Figure 16. In particular, when $\Delta\alpha$ and $\Delta f(\alpha)$ increase and decrease for several times, this indicates that the stress concentration degree is getting higher and higher, and the strain energy is accumulating more and more, which indicates that larger deformation and failure will occur, and it is also regarded as the deformation period. Therefore, reinforcement measures should be taken immediately for the slope to timely control the continuous growth of cracks and prevent the failure of slope deformation and instability.

Compared with conventional monitoring, the monitoring results of displacement meter CX04 (Figure 17(a)) installed at the height of 615 m are shown in Figure 17(b). Since the installation date of CX04 in June 17, the cumulative deformation of the T3301 crack was 1.35 mm, indicating that the deformation of T3301 was in a slow-growing state, that is, in the 'precursor period.' From June 17 to July 8, the cumulative deformation displacement of the T3301 crack was about 6.30 mm. And it was the largest deformation

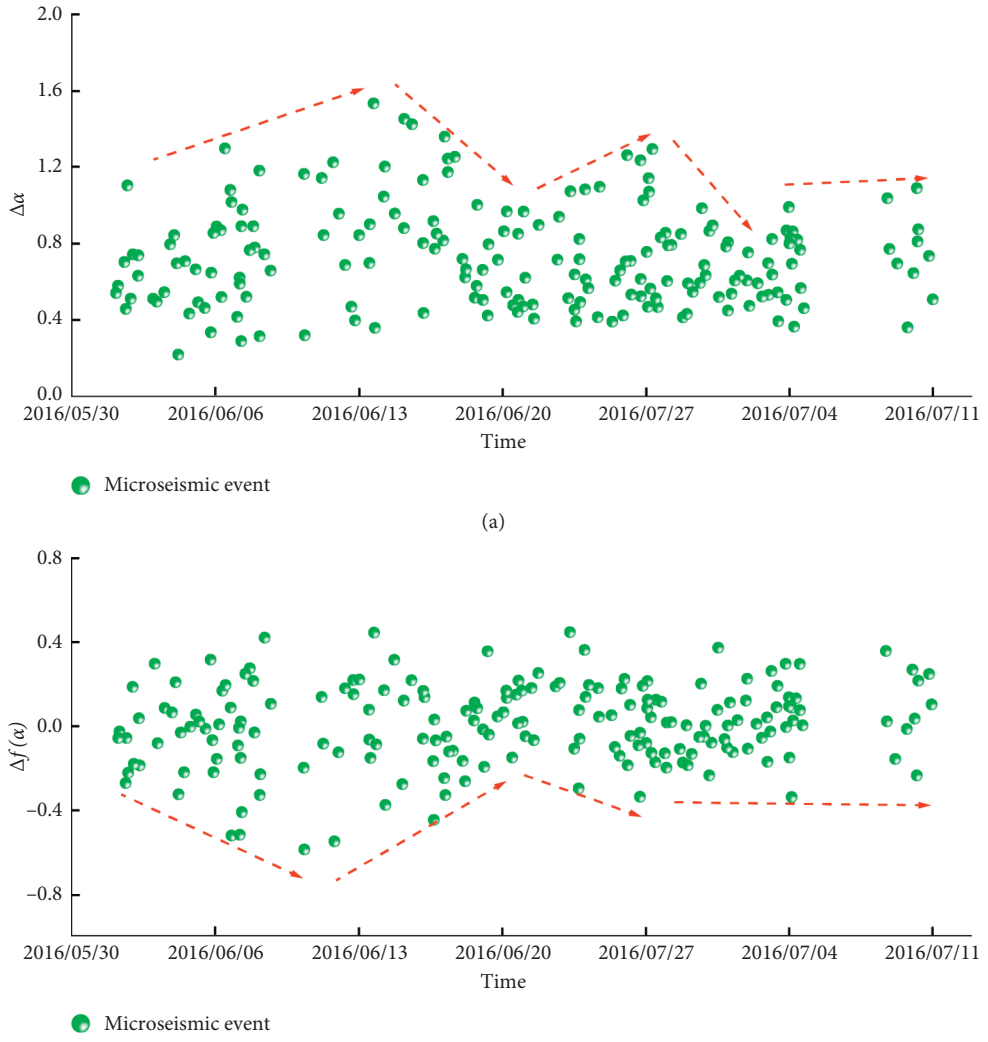

Figure 15: Evolution characteristics of multifractal spectrum parameters vs. time: (a) $\Delta\alpha$ characteristics with time; (b) $\Delta f(\alpha)$ characteristics with time.

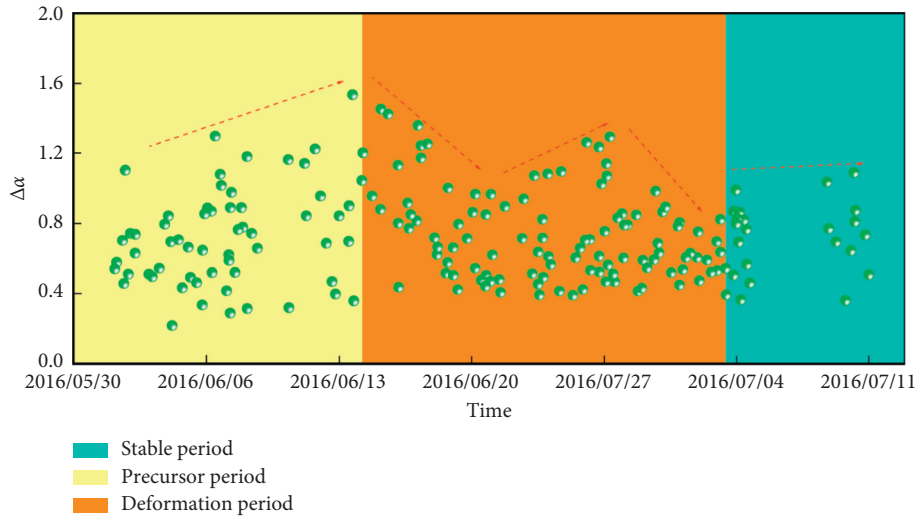

Figure 16: Stage division based on MF-DFA.

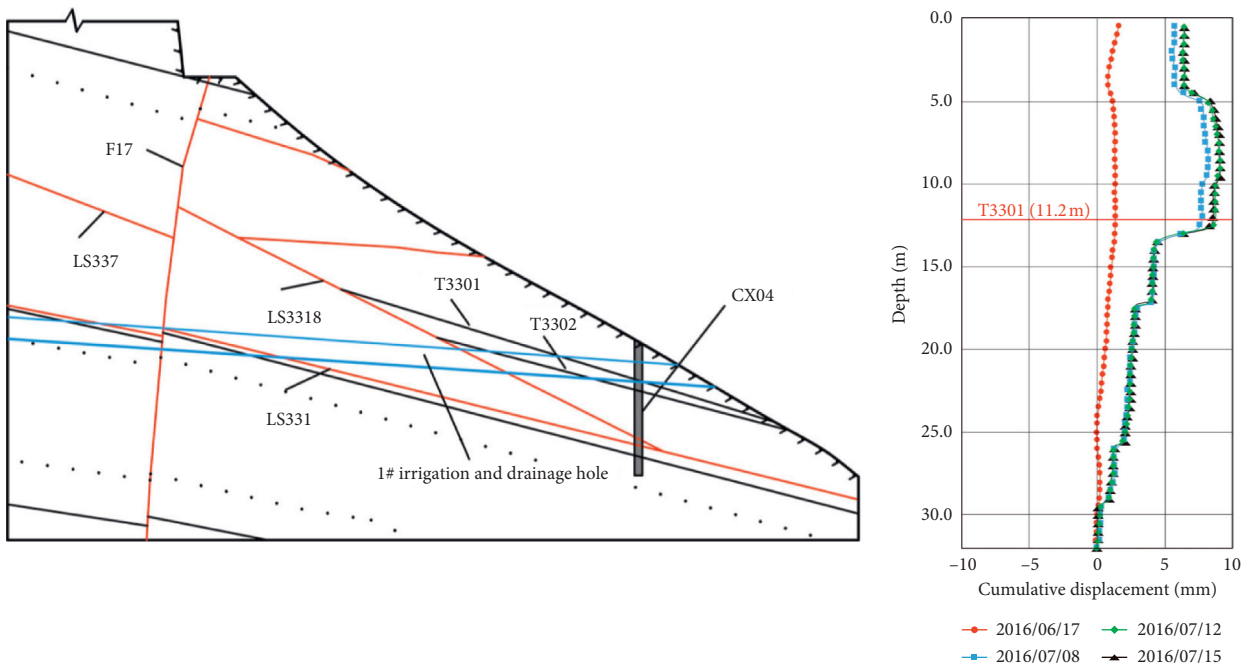

Figure 17: Conventional monitoring result: (a) the location of the CX04, and (b) cumulative displacement data of CX04.

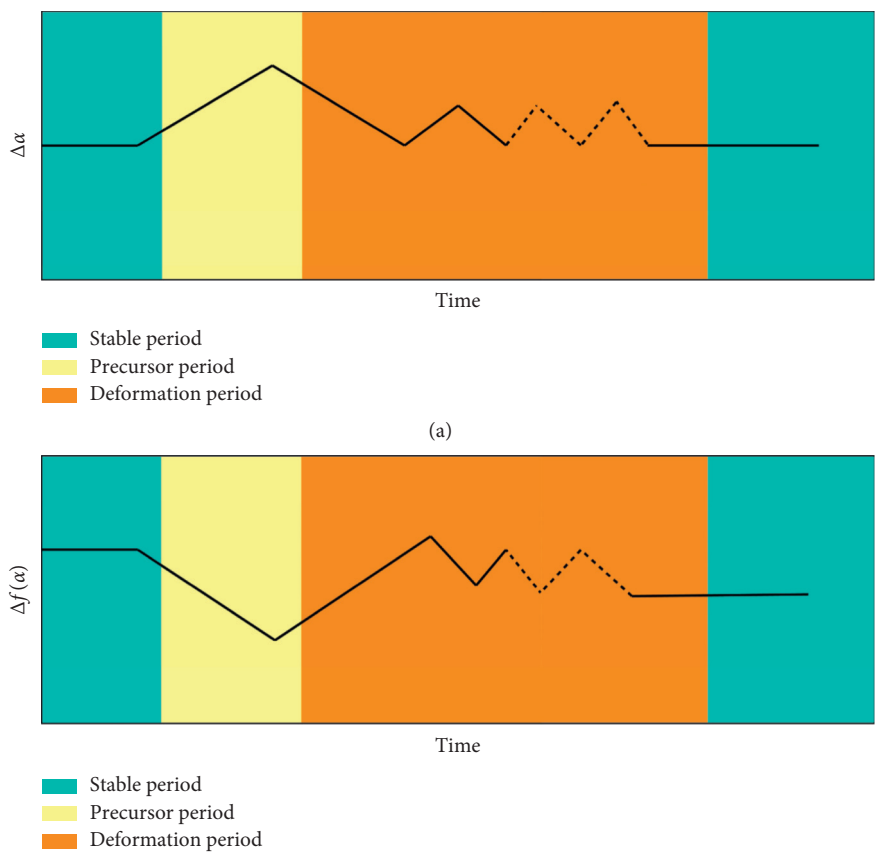

Figure 18: MF-DFA multifractal warning model.

region within the monitoring range of CX04 during the period; the deformation rate reached about 0.3 mm/d; this period was in the 'deformation period.' From July 8 to July 15, the cumulative deformation displacement of the T3301 crack was 0.87 mm, and the average deformation rate was reduced to 0.11 mm/d. And, after July 12, the rock mass had almost no deformation and reached a stable state, which corresponded to the 'stable period.' Combined with field construction, at the end of June and early July, the prestressed anchor cable was installed at the 605–600 m elevation of the dam foundation slope. It enhanced the integrity of the slope rock mass, increased the bearing capacity of the slope rock mass to a certain extent, increased the antisliding friction resistance of the unstable surface, improved the stress adjustment path, effectively controlled the further development of crack, and made the slope rock mass temporarily stable. The early warning analysis of rock slope deformation and failure based on the multifractal time-varying response characteristics of MS signals had a good correspondence with conventional monitoring in time and space. It can accurately describe the mechanical response characteristics of rock slope under the action of excavation unloading. It proves the feasibility of the early warning method of rock slope deformation and failure in this study, which can provide an important reference for rock slope design and safe construction.

6.3. Early Warning Model of Rock Slope Deformation Based on the MF-DFA Method. In actual situations, it is impossible to know when $\Delta\alpha$ and $\Delta f(\alpha)$ reach the peak or valley before large deformation occurs, so the 'precursor period' and 'deformation period' should not be divided at the peak or valley. The warning model is optimized according to the actual situation, as shown in Figure 18. After a period of 'stable period,' $\Delta\alpha$ shows an increasing trend for the first time and $\Delta f(\alpha)$ shows a decreasing trend for the first time, then entering the 'precursory period.' $\Delta\alpha$ reaches the peak and shows a decreasing trend, $\Delta f(\alpha)$ drops to the valley and shows an increasing trend, then the 'precursor period' ends, and the 'deformation period' starts. If $\Delta\alpha$ and $\Delta f(\alpha)$ increase and decrease for several times afterwards, it is still considered to be in the 'deformation period' until the arrival of the next 'stable period.'

7. Conclusion

The MS monitoring technique was adopted to stability analysis of the left bank slope of Baihetan hydropower station. The multifractal characteristics of MS waveforms were carried out based on the MF-DFA method. The following conclusions were drawn.

Based on the MF-DFA method, the multifractal preset parameters of the MS waveform of the left bank slope of Baihetan hydropower station were determined as follows: $s_{\min} = 2^8 = 256$, $s_{\max} = 2^{12} = 4096$, $|q| = 20$, and $m = 3$.

The difference between the multifractal spectrum of typical MS waveform and blasting waveform was obvious: the width of the multifractal spectrum $\Delta\alpha$ of the MS waveform was much smaller than that of the blasting waveform, indicating that the multifractal strength of the blasting waveform was larger and the fluctuation was more intense and complex. The multifractal spectrum $\Delta f(\alpha)$ of the MS waveform was larger than that of the blasting waveform, indicating that small fluctuations in the MS waveform account for a relatively large amount. Furthermore, selecting a waveform with small background noise and large amplitude for analysis can improve the reliability of the multifractal spectrum estimation results.

An early warning model of deformation and failure of rock slope based on MF-DFA was proposed. Before the deformation and failure of surrounding rock mass, $\Delta\alpha$ showed an increasing trend and $\Delta f(\alpha)$ showed a decreasing trend, which can be regarded as 'precursor period;' when deformation and failure occurred, $\Delta\alpha$ showed a decreasing trend and $\Delta f(\alpha)$ showed an increasing trend, which can be regarded as 'deformation period;' after deformation and failure, both $\Delta\alpha$ and $\Delta f(\alpha)$ showed a steady trend, and $\Delta f(\alpha)$ as a whole would be near the zero line, which can be regarded as 'stable period.' Compared to the conventional monitoring data, the early warning model was verified to be feasible. The MF-DFA-based early warning method of rock slope deformation and failure can accurately describe the mechanical response characteristics of rock slope under excavation and unloading.

Data Availability

Some or all data and codes generated or used during the study are available from the corresponding author upon request.

Conflicts of Interest

The authors declare that they have no conflicts of interest regarding the publication of this paper.

Acknowledgments

The authors are grateful for the financial support from the National Natural Science Foundation of China (no. 51679158) and the National Key Research and Development Plan of China (nos. 2018YFC1505004 and 2017YFC1501100).

References

[1] D. T. Bui, H. Moayedi, M. Gör, A. Jaafari, and L. K. Foong, "Predicting slope stability failure through machine learning paradigms," *ISPRS International Journal of Geo-Information*, vol. 8, no. 9, p. 395, 2019.

[2] M. Koopialipoor, D. Jahed Armaghani, A. Hedayat, A. Marto, and B. Gordan, "Applying various hybrid intelligent systems to evaluate and predict slope stability under static and dynamic conditions," *Soft Computing*, vol. 23, no. 14, pp. 5913–5929, 2019.

[3] K. Ma, C.-A. Tang, N.-W. Xu, F. Liu, and J.-W. Xu, "Failure precursor of surrounding rock mass around cross tunnel in high-steep rock slope," *Journal of Central South University*, vol. 20, no. 1, pp. 207–217, 2013.

[4] A. Che, H. Yang, B. Wang, and X. Ge, "Wave propagations through jointed rock masses and their effects on the stability of slopes," *Engineering Geology*, vol. 201, pp. 45–56, 2016.
[5] D. V. Griffiths and G. A. Fenton, "Probabilistic slope stability analysis by finite elements," *Journal of Geotechnical and Geoenvironmental Engineering*, vol. 130, no. 5, pp. 507–518, 2004.
[6] D. V. Griffiths and P. A. Lane, "Slope stability analysis by finite elements," *Géotechnique*, vol. 49, no. 3, pp. 387–403, 1999.
[7] R. Baker and M. Garber, "Theoretical analysis of the stability of slopes," *Géotechnique*, vol. 28, no. 4, pp. 395–411, 1978.
[8] O. Hungr, F. M. Salgado, and P. M. Byrne, "Evaluation of a three-dimensional method of slope stability analysis," *Canadian Geotechnical Journal*, vol. 26, no. 4, pp. 679–686, 1989.
[9] D. J. Sutcliffe, H. S. Yu, and S. W. Sloan, "Lower bound solutions for bearing capacity of jointed rock," *Computers and Geotechnics*, vol. 31, no. 1, pp. 23–36, 2004.
[10] Y. Xiao-Li and Z. A. Liu, "Reliability analysis of three-dimensional rock slope[J]," *Geomechanics and Engineering*, vol. 15, no. 6, pp. 1183–1191, 2018.
[11] N. W. Xu, C. A. Tang, L. C. Li et al., "Microseismic monitoring and stability analysis of the left bank slope in Jinping first stage hydropower station in southwestern China," *International Journal of Rock Mechanics and Mining Sciences*, vol. 48, no. 6, pp. 950–963, 2011.
[12] N.-W. Xu, C.-A. Tang, H. Li et al., "Excavation-induced microseismicity: microseismic monitoring and numerical simulation," *Journal of Zhejiang University Science A*, vol. 13, no. 6, pp. 445–460, 2012.
[13] B. B. Chaudhuri and N. Sarkar, "Texture segmentation using fractal dimension," *IEEE Transactions on Pattern Analysis and Machine Intelligence*, vol. 17, no. 1, pp. 72–77, 1995.
[14] P. Manimaran, P. K. Panigrahi, and J. C. Parikh, "Wavelet analysis and scaling properties of time series," *Physical Review E*, vol. 72, no. 4, Article ID 046120, 2005.
[15] S. Mallat and S. Zhong, "Characterization of signals from multiscale edges," *IEEE Transactions on Pattern Analysis and Machine Intelligence*, vol. 14, no. 7, pp. 710–732, 1992.
[16] J. W. Kantelhardt, S. A. Zschiegner, E. Koscielny-Bunde, S. Havlin, A. Bunde, and H. E. Stanley, "Multifractal detrended fluctuation analysis of nonstationary time series," *Physica A: Statal Mechanics and Its Applications*, vol. 316, no. 1–4, pp. 87–114, 2002.
[17] N. Xu, J. Wu, F. Dai, Y. Fan, T. Li, and B. Li, "Comprehensive evaluation of the stability of the left-bank slope at the Baihetan hydropower station in southwest China," *Bulletin of Engineering Geology and the Environment*, vol. 77, no. 4, pp. 1567–1588, 2018.
[18] X.-B. Wang, K. Jin, and W. Yao, *Report on Engineering Geology of Deformation Treatment of Left Bank Dam Foundation and Dam Abutment Slope at the Elevation of 720-628 M of the Baihetan Hydropower Station along Jinsha River*, p. 147, PowerChina Huadong Engineering Corporation Limited, Hangzhou, China, 2015.
[19] X. Sun, Z.-Q. Wu, and Y. Huang, *Fractal Theory and Its Applications*, pp. 53–88, Science and Technology University Press, Hefei, China, 2003, in Chinese.
[20] E. A. F. Ihlen, "Introduction to multifractal detrended fluctuation analysis in Matlab," *Frontiers in Physiology*, vol. 3, no. 141, p. 141, 2012.
[21] P. Grassberger, "Generalized dimensions of strange attractors," *Physics Letters A*, vol. 97, no. 6, pp. 227–230, 1983.
[22] L. Nan, L. I. Bao-lin, C. Dong, and W.-C. Sun, "Multifractaland time-varying response characteristics of microseismic waves during the rockburst process," *Journal of China University of Mining & Technology*, vol. 46, no. 5, pp. 1007–1013, 2017, in Chinese.
[23] F.-L. Xu, E.-Y. Wang, S. Da-Zhao, S. Xiao-Yan, and W. Ming-Yao, "Long-range correlation and multiracial distribution of acoustic emission of coal-rock," *Rock and Soil Mechanics*, vol. 32, no. 7, pp. 2111–2116 + 2122, 2011, in Chinese.
[24] F. Xia-Ting, C. Bing-Rui, H.-J. Ming, S.-Y. Wu, and X. Ya-Xun, "Evolution law and mechanism of rockbursts in deep tunnels:immediate rockburst," *Chinese Journal of Rock Mechanics and Engineering*, vol. 31, no. 3, pp. 561–569, 2012, in Chinese.